

Bistability of Slow and Fast Traveling Waves in Fluid Mixtures

St. Hollinger, P. Büchel, and M. Lücke

Institut für Theoretische Physik, Universität des Saarlandes, Postfach 151150, D66041 Saarbrücken, Germany

(Received 2 July 1996)

The appearance of a new type of fast nonlinear traveling wave states in binary fluid convection with increasing Soret effect is elucidated and the parameter range of their bistability with the common slower ones is evaluated numerically. The bifurcation behavior and the significantly different spatiotemporal properties of the different wave states—e.g., frequency, flow structure, and concentration distribution—are determined and related to each other and to a convenient measure of their nonlinearity. This allows one to derive a limit for the applicability of small amplitude expansions. Additionally, a universal scaling behavior of frequencies and mixing properties is found. [S0031-9007(96)02101-1]

PACS numbers: 47.20.Ky, 03.40.Kf, 47.10.+g

In binary fluid mixtures heated from below, there is an interesting feedback loop between the fields of concentration, velocity, and temperature. The buoyancy force that drives the convective flow is changed by concentration variations. They, in turn, are *produced* via the Soret effect [1,2] by temperature gradients, i.e., via thermodiffusion and *reduced* by dissipative concentration diffusion and by mixing through the convective flow. This coupling chain causes a surprising richness of spatiotemporal pattern formation [3] even close to the onset of convection. In particular, there are convective structures [2–15] consisting of coupled traveling waves (TW's) of velocity, temperature, and concentration with significantly different shapes [14,15]. Since nonlinear concentration advection is typically much larger than linear diffusion—the ratio of these two transport rates can easily be above 1000—it is not surprising that these TW states are typically strongly nonlinear.

In this Letter we elucidate how with increasing Soret coupling there appear two different bistable TW's—one about twice as fast as the other—which both stably coexist with the stable quiescent conductive state. The convective amplitude of the fast (slow) TW is small (large) while the amplitude of its concentration contrast is large (small). The fast stable TW's have so far remained unnoticed in experiments [4–13] and numerical simulations [14,15]. They develop with increasing Soret coupling via a saddle node bifurcation out of a dent in the subcritically bifurcating unstable TW branch. They are most easily accessible via a two-loop hysteresis at larger but experimentally realizable Soret effects. Furthermore, we discovered an universal scaling behavior of TW frequencies and mixing properties. We also found that the ratio of flow and phase velocity is a relevant parameter and a convenient measure of their nonlinearity that allows one to determine where an amplitude expansion around the onset breaks down.

To investigate roll-like convection structures in a horizontal layer of, say, ethanol water with Lewis number $L = 0.01$ and Prandtl number $\sigma = 10$, we determine the convective solutions that bifurcate with a lateral periodic-

ity length $\lambda = 2$ out of the quiescent heat conducting state [16]. A finite difference method [17] as well as a many mode Galerkin scheme is used to solve the appropriate field equations [1,15] in a vertical cross section through the rolls perpendicular to their axes. Horizontal boundaries at top and bottom, $z = \pm 1/2$, are no slip, perfectly heat conducting, and impermeable. Our control parameter $r = R/R_c^0$ measuring the thermal driving is the Rayleigh number R reduced by the critical one $R_c^0 = 1707.762$ for the onset of convection in a pure fluid. We are interested here in negative separation ratios ψ [3]. Then the Soret coupling between deviations T of temperature and C of concentration from their means tends to increase (decrease) the ethanol concentration in the cold (warm) fluid regions.

In Fig. 1 we show how an increasing Soret coupling strength changes the bifurcation diagrams of (a) maximal vertical flow intensity w_{\max}^2 , (b) TW frequency ω , (c) mixing number $1 - M$, and (d) convective contribution $N - 1$ to the Nusselt number. The order parameter $1 - M = 1 - \sqrt{\langle C^2 \rangle / \langle C_{\text{cond}}^2 \rangle}$ measures the convective mixing. It is defined so as to vanish in the conductive state, $C_{\text{cond}} = -\psi z$, and it approaches +1 for convection with strong mixing properties where the spatially averaged square of the concentration variation $\langle C^2 \rangle$ becomes small. The overall subcritical bifurcation topology is caused by the interplay of two adverse effects: (i) The Soret coupling to the degrees of freedom of the concentration field stabilizes the quiescent basic state [19], since the Soret induced concentration distribution reduces the buoyancy force that drives convection. This shifts with increasing $|\psi|$ the TW bifurcation threshold r_{osc} (arrows in Fig. 1) upward along the r axis. (ii) With increasing convection mixing advectively reduces the Soret induced concentration gradients and with it the influence of the Soret effect on the buoyancy so that the convection behavior of the mixture approaches that of the pure fluid—dashed curves labelled $\psi = 0$ in Figs. 1(a) and 1(d).

We found that the spatiotemporal properties of TW states substantially change when the convective flow w_{\max} becomes larger than the phase velocity $v = \omega \frac{\lambda}{2\pi}$. Starting at r_{osc} with a large Hopf frequency ω_H and $w_{\max} = 0$,

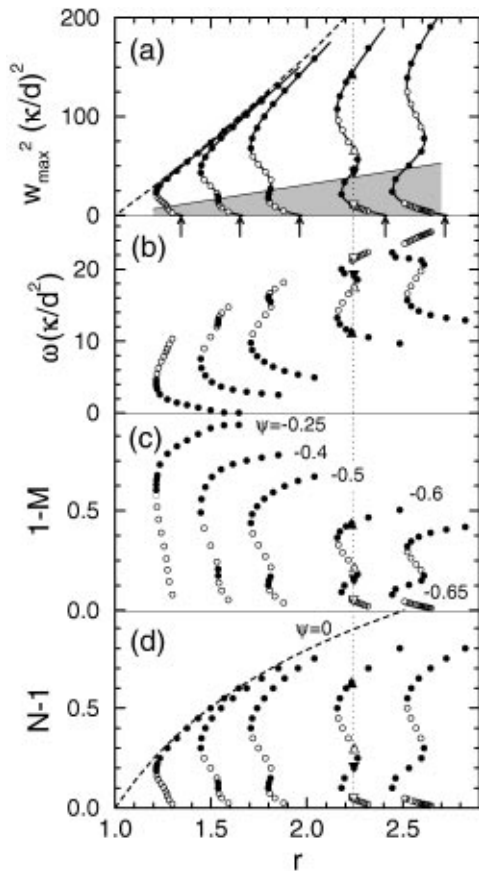


FIG. 1. Evolution of TW-bifurcation diagrams with Soret coupling strength ψ : (a) squared maximal vertical flow w_{\max}^2 , (b) frequency ω , (c) mixing number $1 - M$, and (d) convective contribution to the Nusselt number $N - 1$ vs reduced Rayleigh number r . Stable (unstable) TW states are marked by filled (open) symbols. Four of them on the vertical dotted line at $r = 2.24$, $\psi = -0.6$ are identified for later discussion by different triangles. Arrows mark Hopf thresholds for onset of TW convection. The $\psi = 0$ pure fluid limit is included in (a) and (d) by the dashed line. Full lines through the data points of (a) represent the fit discussed in the text. Only states in the shaded region of (a) are weakly nonlinear (cf. text).

the frequency [Fig. 1(b)] monotonically decreases along the TW solution branch while the convection amplitude w_{\max} grows. States with $\chi = w_{\max}/\nu < 1$ [shaded region in Fig. 1(a)] are weakly nonlinear, while those with larger χ are strongly nonlinear. In the former there are only open streamlines in the frame comoving with the TW [Fig. 2(a)] and the concentration wave profile is basically harmonic [Fig. 2(b), ∇ and \blacktriangledown]. On the other hand, for $\chi > 1$ there are also regions of closed streamlines [Fig. 2(c)]. With growing χ their size and with it the anharmonicity of the concentration wave [Fig. 2(b), \triangle and \blacktriangle] increases, since within regions of closed streamlines concentration is diffusively mixed to alternatingly high and low plateau levels. Moving along a TW branch, one observes with growing χ first an increase of the amplitude of a harmonic concentration wave up to $\chi \approx 1$ and then

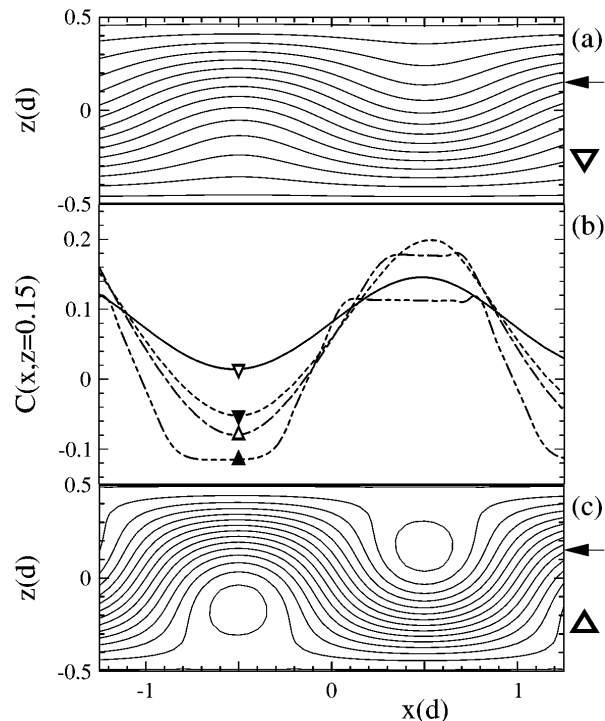


FIG. 2. (b) Wave profiles of concentration deviation C (scaled by $\Delta T \alpha / \beta$) at the vertical position marked by arrows in (a) and (c). Therein streamlines in the frame comoving with the TW are shown. Symbols identify states in Fig. 1 on the dotted vertical line.

a decrease in amplitude combined with its wave profile becoming more and more trapezoidal [Fig. 2(b)].

The structural changes that occur with growing χ can be observed experimentally in topview and even better in sideview shadowgraph intensity distributions [10,12,20]. The sideviews in Fig. 3 of four TW's (marked by triangles in Fig. 1) existing at the same $r \approx 2.24$ show in Fig. 3(a) the smooth distribution of a weakly nonlinear linear state (∇) and in Figs. 3(b)–3(d) strongly nonlinear ones. In the latter the Soret induced ethanol rich (poor) boundary layers near the top (bottom) plate increasingly discharge via concentration jets into the growing roll-like regions of closed streamlines. Therein, the concentration is then homogenized on alternating high and low levels.

With increasing Soret coupling strength $|\psi|$, the TW solution branches in Fig. 1 become more and more contorted. Already at $\psi \approx -0.001$ the lower unstable branches of w_{\max}^2 and N have two inflection points with a dent in-between that can clearly be seen in Fig. 1 at $\psi = -0.25$. The significance of such a dent on the lower unstable branch of solutions being inaccessible to experiments [4–13] as well as to earlier numerical simulations [14,15] has not been appreciated appropriately, although it can be seen in the paper of Bensimon et al. [21] in the limit of small Soret coupling and $\sigma \rightarrow \infty$. With our new finite difference method and our many mode Galerkin scheme, we can now trace out the complete

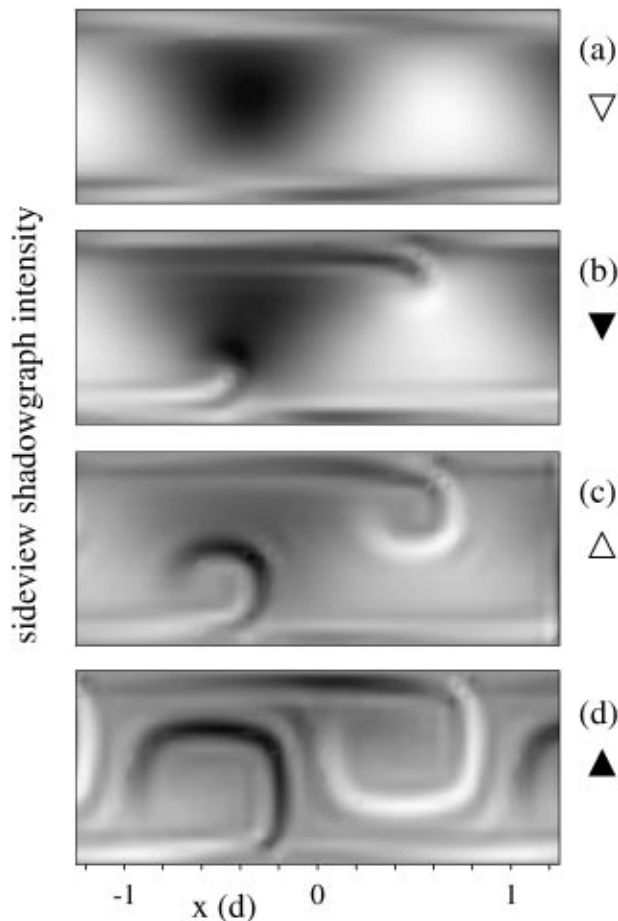


FIG. 3. Sideview shadowgraph intensity distributions obtained as described in [10,15] from the numerically determined TW states that are marked by the respective triangles in Fig. 1.

solution branch and determine how its bifurcation topology changes with ψ . We found that the above mentioned dent develops at $\psi \approx -0.4$ into a forward bending arc when the first inflection point (* in Fig. 4) emits two new saddles (■ and • in Fig. 4). So in the shaded region of the control parameter plane of Fig. 4, three stable states occur: For $\psi \lesssim -0.4$ two different stable TW's coexist—one fast, the other one slow—that compete with each other and with the stable quiescent basic state. Furthermore, a new scenario appears for $\psi \lesssim -0.61$. There, the Rayleigh number r_{osc}^S of the saddle with small N , w_{max} and large ω drops below the saddle r_{osc}^L with large N , w_{max} and small ω so that a two-step hysteresis opens up between basic state, slow TW's, and fast TW's [22].

The first inflection point (* in Fig. 4) of the TW bifurcation branch coincides closely with the boundary $\chi = 1$ between weakly and strongly nonlinear states—the change in curvature of the bifurcation branch reflects the change in the TW structure. Even for ψ as small as about -0.001 amplitude equations of quintic order might possibly reproduce realistically only those TW states that lie between r_{osc} and the first inflection point. The fact that $\chi \approx 1$ is an upper limit to amplitude expansions around

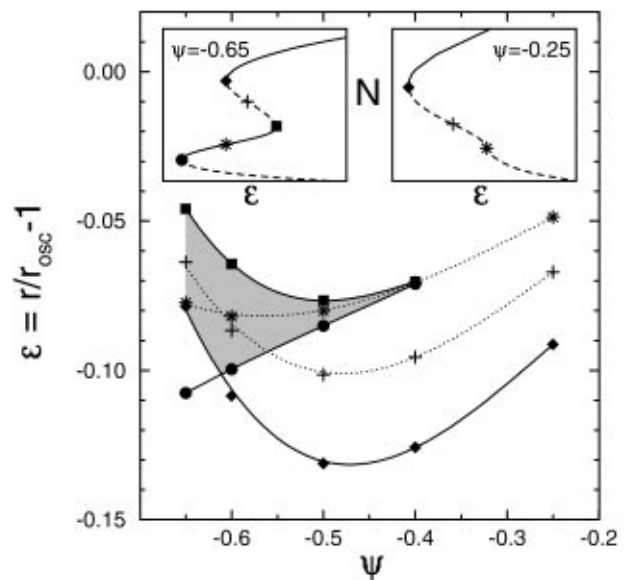


FIG. 4. $\psi - \epsilon$ phase diagram of TW states at subcritical driving. In the shaded parameter regime two stable TW's exist. Bifurcation diagrams of N vs ϵ in the insets explain the meaning of the symbols: •, ■, and ◆ represent saddle node states with small, medium, and large convection amplitude (large, medium, and small frequency), respectively. The first (second) inflection point is denoted by * (+).

the Hopf bifurcation threshold follows also directly from the behavior of the multivalued functional dependence of the flow intensity $X = w_{max}^2$ on r . Its singlevalued inverse $r(X)$ —to see it just turn Fig. 1(a) by 90° —can be represented extremely well by the product

$$r(X) = r_0(X) Q(X), \quad (1)$$

cf. the full lines in Fig. 1(a). Here $r_0(X)$ is the $\psi = 0$ border curve for the pure fluid [dashed line in Fig. 1(a)] that starts at $r_0(X = 0) = 1$ and grows for large X slightly sublinearly. The rational function

$$Q(X) = \frac{a_0 + a_1X + a_2X^2 + a_3X^3}{1 + b_1X + b_2X^2 + b_3X^3}$$

ensures with $a_0 = r_{osc}$ that $r(X = 0) = r_{osc}$ and with finite a_3/b_3 that $r - r_0$ does not diverge for large X . With the third order polynomials in Q , four different X can have the same r . In that sense (1) is a minimal representation of the bifurcation diagrams of Fig. 1(a). Now, the radius of convergence X_c of an amplitude expansion of Q in a power series in X is given by the absolute value of that pole of Q closest to $X = 0$ in the complex X plane. Our fits for $Q(X)$ show that this pole lies on the negative real X -axis with X_c close to v^2 so that $\chi = w_{max}/v \approx 1$ is indeed an *upper limit* for the applicability of amplitude expansions.

A recent TW model [23] into which χ enters as a relevant parameter predicts that the frequencies are

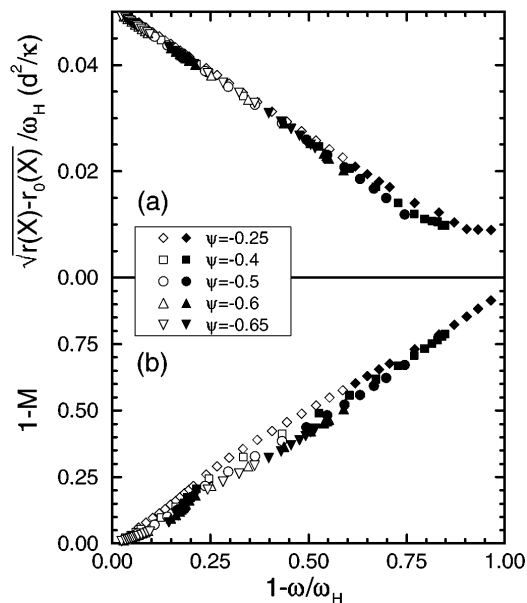


FIG. 5. Universal, ψ independent scaling relations between: (a) frequency and “distance” $r - r_0$ of TW states from $\psi = 0$ convection (cf. text), (b) degree of convective mixing $1 - M$ and TW frequency. Here ω_H is the Hopf frequency at onset. Shown are all TW states of Fig. 1 and some that have been suppressed there for clarity (stable TW’s—filled symbols; unstable TW’s—open symbols).

universally determined by the “distance” $r(X) - r_0(X)$ of the TW states from the pure fluid convection state ($\psi = 0$). For any TW with a particular $X = w_{\max}^2$, this distance parallel to the r -axis can be read off in Fig. 1(a). We confirm this prediction in Fig. 5(a). It shows that the scaled frequencies $1 - \omega/\omega_H$ are indeed linearly related to $\sqrt{r - r_0}/\omega_H$ in a universal, ψ -independent manner that holds for stable as well as for unstable TW’s. Furthermore, according to Fig. 5(b), the convective mixing $1 - M$ grows linearly with the reduced frequency deviation $1 - \omega/\omega_H$ from the Hopf frequency and also $1 - M$ is roughly linearly related to $\sqrt{r - r_0}/\omega_H$.

To summarize, we have found bistability between slow and fast TW’s and we have elucidated how the latter appear when the Soret coupling becomes sufficiently strong. Test runs with smaller Lewis and/or larger Prandtl numbers lead to similar bifurcation behavior. To check our results experimentally—preferably in annular containers—and also to investigate effects related to spatially confined states, we suggest using mixtures with $\psi \approx -0.6$ as in Refs. [4,5].

This work was supported by the Deutsche Forschungsgemeinschaft. A graduate scholarship of the Saarland for one of us (SH) is gratefully acknowledged.

[1] L. D. Landau and E. M. Lifshitz, *Fluid Mechanics* (Pergamon Press, Oxford, 1959).

[2] J. K. Platten and J. C. Legros, *Convection in Liquids* (Springer-Verlag, Berlin, 1984).

- [3] M. C. Cross and P. C. Hohenberg, *Rev. Mod. Phys.* **65**, 851 (1993).
- [4] R. W. Walden, P. Kolodner, A. Passner, and C. M. Surko, *Phys. Rev. Lett.* **55**, 496 (1985).
- [5] H. Touiri, J. K. Platten, and G. Chavepeyer, *Eur. J. Mech., B/Fluids* **15** (2), 241 (1996).
- [6] G. Ahlers and I. Rehberg, *Phys. Rev. Lett.* **56**, 1373 (1986).
- [7] H. Gao and R. P. Behringer, *Phys. Rev. A* **34**, 697 (1986).
- [8] E. Moses and V. Steinberg, *Phys. Rev. Lett.* **60**, 2030 (1988).
- [9] D. R. Ohlsen, S. Y. Yamamoto, C. M. Surko, and P. Kolodner, *Phys. Rev. Lett.* **65**, 1431 (1990).
- [10] K. D. Eaton, D. R. Ohlsen, S. Y. Yamamoto, C. M. Surko, W. Barten, M. Lücke, M. Kamps, and P. Kolodner, *Phys. Rev. A* **43**, 7105 (1991).
- [11] G. Zimmermann and U. Müller, *Int. J. Heat Mass Transfer* **35**, 2245 (1992).
- [12] B. L. Winkler and P. Kolodner, *J. Fluid Mech.* **240**, 31 (1992).
- [13] A. La Porta, K. D. Eaton, and C. M. Surko, *Phys. Rev. E* **53**, 570 (1996).
- [14] W. Barten, M. Lücke, W. Hort, and M. Kamps, *Phys. Rev. Lett.* **63**, 376 (1989).
- [15] W. Barten, M. Lücke, M. Kamps, and R. Schmitz, *Phys. Rev. E* **51**, 5636 (1995).
- [16] We scale lengths by the thickness d of the fluid layer, times by the vertical diffusion time d^2/κ , deviations T from the mean temperature by the imposed vertical temperature difference ΔT , and deviations C from the mean concentration by $\Delta T \alpha/\beta$ with α (β) being the thermal (solubility) expansion coefficient. $L = D/\kappa$ is the Lewis number and $\sigma = \nu/\kappa$ the Prandtl number. Here ν is the kinematic viscosity, κ the thermal diffusivity, and D the concentration diffusion coefficient.
- [17] We use a finite difference algorithm [15] that is modified by a multigrid method for pressure iteration and a DuFort-Frankel scheme to solve the momentum balance equations [18]. The unstable TW solutions are determined with a linear control process in which the temperatures at the plates are varied.
- [18] Ch. Jung, private communication.
- [19] D. T. J. Hurle and E. Jakeman, *J. Fluid Mech.* **47**, 667 (1971); E. Knobloch and D. R. Moore, *Phys. Rev. A* **36**, 860 (1988); M. C. Cross and K. Kim, *Phys. Rev. A* **37**, 3909 (1988).
- [20] P. Kolodner, H. L. Williams, and C. Moe, *J. Chem. Phys.* **88**, 6512 (1988).
- [21] D. Bensimon, A. Pumir, and B. I. Shraiman, *J. Phys. (France)* **50**, 3089 (1989).
- [22] The fast stable TW’s in this paper are genuine extended states that occur only for sufficiently strong Soret coupling. They are unrelated to the weakly nonlinear fast waves shown schematically in Ref. [3], Fig. 53. The latter appear even for small $|\psi|$, but only in finite-length nonannular convection channels with lateral endwalls that have a finite reflectivity for convection perturbations. See also V. Steinberg, J. Fineberg, E. Moses, and I. Rehberg, *Physica (Amsterdam)* **37D**, 359 (1989).
- [23] St. Hollinger and M. Lücke (to be published).